

Coordinated primary frequency control among non-synchronous systems connected by a multi-terminal high-voltage direct current grid

J. Dai¹ Y. Phulpin² A. Sarlette³ D. Ernst⁴

¹Department of Power and Energy Systems, SUPELEC, 3, rue Joliot Curie, 91192 Gif-sur-Yvette, France

²INESC Porto, Rua Dr. Roberto Frias 378, 4200-465 Porto, Portugal

³SYSTeMS, Gent University, Technologiepark Zwijnaarde 914, 9052 Zwijnaarde (Gent), Belgium

⁴Department of Electrical Engineering and Computer Science, University of Liège, B-4000 Liège, Belgium

E-mail: jing.dai@supelec.fr

Abstract: The authors consider a power system composed of several non-synchronous AC areas connected by a multi-terminal high-voltage direct current (HVDC) grid. In this context, the authors propose a distributed control scheme that modifies the power injections from the different AC areas into the DC grid so as to make the system collectively react to load imbalances. This collective reaction allows each individual AC area to downscale its primary reserves. The scheme is inspired by algorithms for the consensus problem extensively studied by the control theory community. It modifies the power injections based on frequency deviations of the AC areas so as to make them stay close to each other. A stability analysis of the closed-loop system is reported as well as simulation results on a benchmark power system with five AC areas. These results show that with proper tuning, the control scheme makes the frequency deviations converge rapidly to a common value following a load imbalance in an area.

1 Introduction

The frequency of an AC power system varies when there is an imbalance between the produced and the consumed amounts of power. To maintain the frequency of a power system close to its nominal value, system operators have developed frequency control schemes, which are usually classified according to the time scale of their actions [1]. The actions corresponding to the shortest time scale are usually referred to as ‘primary frequency control’. It consists of automatic adjustment, within a few seconds after a power imbalance, of the generators’ power output based on locally measured frequency variations. To this end, the generators must have power margins that can be rapidly deployed, that is, primary frequency control reserves.

The frequency averaged over a few seconds can be considered identical in any part of a synchronous area. With a common frequency, every generator participating in primary frequency control adjusts its generation output in response to frequency excursions in the synchronous area, regardless of the location of the power imbalances. As the efforts of these generators sum up within a synchronous area, larger systems usually experience smaller frequency deviations. In addition, given that the size of the primary reserves required in a system is usually determined by the single network element whose loss would have the greatest impact on network power balance, larger systems also have more consumers to bear the consequence of the loss of that

single element, which implies lower operational costs – per MWh produced – associated to the provision of primary reserves. This has been a significant motivation for interconnecting regional and national systems to create large-scale power systems, such as the UCTE network.

The development of high-voltage direct current (HVDC) systems for bulk power transmission over long distances [2] and underground cable crossings opens new perspectives for interconnecting non-synchronous areas. In this context, it is generally expected that the power flows through an HVDC system are set at scheduled values, whereas the frequencies of the AC areas remain independent. This type of HVDC control scheme may prevent the system from cascading outages by limiting the effects of a severe contingency within one area [3]. It also makes sense when the interconnected transmission utilities cannot agree on a common practice in terms of frequency control. However, this control scheme prevents the primary reserves from being shared among the non-synchronous AC areas, as the generators in one area are insensitive to frequency excursions in other areas. Since the supply of primary reserves represents a significant part of the operational transmission costs [4], it would be economically advantageous to share primary reserves among the non-synchronous areas by making use of the fast power-tracking capability of HVDC converters.

Hence, the use of HVDC for primary frequency control has been considered in [5, 6] for a system with two AC areas.

In these references, it is suggested to add to the scheduled power flow setting, a term that is proportional to the frequency difference between the two areas. Simulation results provided in both papers show that such frequency feedback control leads to smaller frequency differences between the two areas. Furthermore, de Toledo *et al.* [5] also mention that using HVDC for primary frequency control yields reduced costs of primary reserves.

The present paper proposes and studies a distributed control scheme to share the primary reserves among an arbitrary number of non-synchronous AC areas connected by a multi-terminal HVDC (MT-HVDC) system. Although the control laws proposed in [5, 6] were heuristically designed, our control scheme is derived from algorithms for the extensively studied consensus problem, which appears in the context of coordination of multi-agent systems [7]. With the proposed scheme, the power injections from the AC areas into the DC grid are coordinated in such a way that the frequency deviations of all the AC areas stay close to each other despite power imbalances in one area. Thus, this control scheme makes it possible to decrease the necessary amount of primary reserves for the entire system, as if the AC areas were interconnected through an AC grid. Theoretically, this control scheme can be applied to both thyristor-based HVDC systems and voltage–source–converter (VSC)-based HVDC systems. However, as thyristor-based HVDC converters necessitate adequate reactive power support, VSC would be a more appropriate technology thanks to its independent control on real and reactive power.

The paper is organised as follows. Section 2 describes primary frequency control and proposes a model of an MT-HVDC system. Section 3 formulates the control objective and proposes a distributed control scheme. Section 4 analyses stability of the controlled system. Section 5 gathers simulation results on a five-area system. Section 6 concludes.

2 Primary frequency control in an MT-HVDC system

In this section, we first describe the mechanism of primary frequency control of one generator, from which the notion of primary reserve arises. Then, a model for studying frequency deviations in a MT-HVDC system is proposed.

2.1 Primary frequency control and primary reserve

A generator that participates in primary frequency control is equipped with a speed governor, which observes the shaft's rotating speed, and uses a servomotor to control a throttle that determines the amount of fluid sent to the turbine [8]. When the speed governor detects a deviation of the generator rotational speed, which is proportional to the stator electrical frequency f , its servomotor adjusts the opening of the throttle valve within a few seconds, thereby modifying the power input to the generator P_m .

When the frequency is equal to its nominal value f_{nom} , P_m equals its reference value P_m^o . As P_m^o is set by secondary frequency control within a period of about 30 s [1], we assume in this paper that P_m^o remains constant.

The dynamics of primary frequency control are expressed as

$$T_{sm} \frac{dP_m}{dt} = P_m^o - P_m - \frac{P_{nom} f - f_{nom}}{\sigma f_{nom}} \quad (1)$$

where T_{sm} is the time constant of the servomotor, σ is the generator droop, and P_{nom} the rated mechanical power of the generator.

The limits on P_m , denoted by P_m^{\min} and P_m^{\max} , are imposed by technical and economic attributes of the generator. The quantity $P_m^{\max} - P_m^o$ is referred to as 'primary reserve'.

2.2 MT-HVDC system model

To study frequency variations in an MT-HVDC system, we consider the system represented in Fig. 1. The system has three types of components: a DC grid, N non-synchronous AC areas and N converters that interface the AC areas with the DC grid.

2.2.1 DC grid: As the electrical time constant of a DC grid is of the order of a few milliseconds [9], transient dynamics of the DC grid are not considered hereafter.

To take into account the general case where all the nodes are not connected to an AC area, we suppose that there are in total $M \geq N$ nodes in the DC grid and that node i is connected to AC area i via converter i , $\forall i \in \{1, \dots, N\}$. Then, the power transferred from node i to node j within the DC network, denoted by P_{ij}^{dc} , can be expressed as

$$P_{ij}^{dc} = \frac{V_i^{dc}(V_i^{dc} - V_j^{dc})}{R_{ij}} \quad (2)$$

where V_i^{dc} and V_j^{dc} are the voltages at nodes i and j , respectively, and R_{ij} is the resistance between these two nodes. If nodes i and j are not directly connected, R_{ij} is considered equal to infinity. Note that there must be either a direct or an indirect connection between any two nodes, otherwise the DC grid would be made of several parts disconnected from each other.

Let P_i^{dc} denote the power injection from AC area i into the DC grid. Then, the power balance at node i satisfies

$$\sum_{j \neq i} P_{ij}^{dc} = \begin{cases} P_i^{dc} & \text{for } i \leq N \\ 0 & \text{for } i > N \end{cases} \quad (3)$$

By replacing P_{ij}^{dc} by (2), we can write (3) in matrix form

$$\mathbf{P}^{dc} = \text{diag}(V_1^{dc}, \dots, V_M^{dc}) \mathbf{A} \mathbf{V}^{dc} \quad (4)$$

where \mathbf{P}^{dc} is a vector of length M with the first N components equal to $P_1^{dc}, \dots, P_N^{dc}$ and the last $M-N$ components equal to 0, \mathbf{V}^{dc} is a vector containing the DC voltages $V_1^{dc}, \dots, V_M^{dc}$.

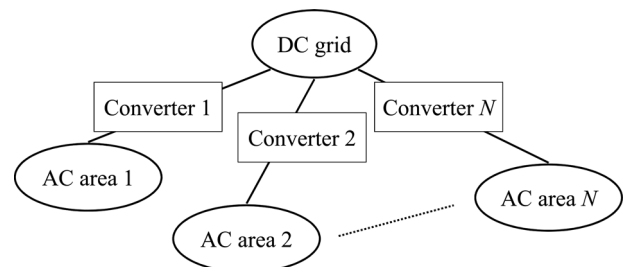


Fig. 1 MT-HVDC system connecting N AC areas via N converters

The components of matrix A are defined as

$$[A]_{ij} = \begin{cases} -\frac{1}{R_{ij}} & \text{for } i \neq j \\ \sum_{j \neq i} \frac{1}{R_{ij}} & \text{for } i = j \end{cases}$$

Given a connected matrix A , (4) has a unique solution once the voltage V^{dc} of a node and the power injections P^{dc} of the other nodes are fixed.

2.2.2 AC areas: An AC area in a real HVDC system usually contains a large number of generators. In our study on primary frequency control, whose time scale is several seconds, the frequency can be considered identical in any part of the AC area. Thus, we use an aggregated model to represent the mechanical dynamics of all the generators within the area. Aggregation methods such as the one in [10] can be used to find the parameters of the aggregated generator.

On the one hand, the evolution of the frequency is determined by the equation of motion for area i as

$$2\pi J_i \frac{df_i}{dt} = \frac{P_{mi} - P_{ei}}{2\pi f_i} - 2\pi D_{gi}(f_i - f_{\text{nom},i}) \quad (5)$$

where f_i is the frequency of area i , and $f_{\text{nom},i}$ its nominal value; P_{mi} and P_{ei} are the mechanical power input and the electrical power output of the aggregated generator for area i , respectively; J_i and D_{gi} are the moment of inertia and the damping factor of this generator. On the other hand, in response to frequency excursions, the speed governor of the aggregated generator adjusts its mechanical power input P_{mi} according to (1).

The loads within an area are also aggregated and their sum, denoted by P_{li} , is represented by a static load model [11]

$$P_{li} = P_{li}^o \cdot (1 + D_{li}(f_i - f_{\text{nom},i})) \quad (6)$$

where P_{li}^o is the value of P_{li} when $f_i = f_{\text{nom},i}$, and D_{li} is the frequency sensitivity factor.

Finally, the power balance within area i requires that

$$P_{ei} = P_{li} + P_i^{\text{dc}} \quad (7)$$

2.2.3 Converters: Conventionally, in an MT-HVDC system, only one of the converters regulates the DC voltage, whereas all the others control the power exchanged between the AC and the DC sides [12–14]. In fact, the converter regulating the DC voltage plays the role of the slack bus that maintains the power balance within the DC grid, and the latter can be considered as a power exchange centre between the different AC areas. Without loss of generality, we assume that it is the converter connected to area N that regulates the DC voltage.

Formally, with the notations introduced in Section 2.2.1, $P_1^{\text{dc}}, \dots, P_{N-1}^{\text{dc}}$ can be used as control variables to achieve a control objective, whereas P_N^{dc} is determined by the DC grid load flow to maintain the power balance within the DC grid, that is, the value of P_N^{dc} corresponds to the single value satisfying (4) for given $P_1^{\text{dc}}, \dots, P_{N-1}^{\text{dc}}$ and V_N^{dc} .

2.3 Events leading to frequency excursions

A frequency excursion results from a power imbalance, which may originate from a variation in demand or generation. The most common events consist of continual variations in the load demand P_{li}^o , which require that the generation utilities taking part in frequency regulation continually adjust their output. For such types of events, the aggregated generator inertia J_i and the reserve $P_{mi}^{\text{max}} - P_{mi}^o$ of each area are usually considered unchanged. More rarely, a sudden loss of a generator also results in a power imbalance. In this case, the inertia and the reserve of the AC areas change.

For the sake of simplicity, in the theoretical and the experimental studies reported later in this paper, we will only consider demand-related imbalances. More specifically, we will study the effects, on our controlled system dynamics, of a step change in the load demand of one of the AC areas. This step response analysis is sufficient to characterise system behaviour in more general conditions (at very least, by the superposition principle, for the linearised system).

3 Distributed control scheme

In this section, we propose a distributed control scheme that shares primary reserves among non-synchronous AC areas.

3.1 Control objective

To make every generator sensitive to a system-wide power imbalance, the frequency of every AC area must reflect the overall generation/demand balance of the entire system. This can be achieved by making the frequency deviations of all areas follow each other at any time. Thus, our objective is to design a control scheme that makes equal the frequency deviations of all the areas.

The control variables are the power injections $P_1^{\text{dc}}, \dots, P_{N-1}^{\text{dc}}$. They are modulated under the following constraints

$$P_i^{\text{dc}, \min} \leq P_i^{\text{dc}} \leq P_i^{\text{dc}, \max}, \quad \forall i \in \{1, \dots, N\} \quad (8)$$

$$V_i^{\text{dc}, \min} \leq V_i^{\text{dc}} \leq V_i^{\text{dc}, \max}, \quad \forall i \in \{1, \dots, M\} \quad (9)$$

where $P_i^{\text{dc}, \min}$ and $P_i^{\text{dc}, \max}$ ($V_i^{\text{dc}, \min}$ and $V_i^{\text{dc}, \max}$, resp.) are the minimum and the maximum acceptable values of P_i^{dc} (V_i^{dc} , resp.). In practice, these values depend on both the technological characteristics of converter i and the DC voltages of the other converters in the DC grid. Indeed, appropriate $V_i^{\text{dc}, \min}$ and $V_i^{\text{dc}, \max}$ are meant to ensure that the transmission limits of the DC lines and the power ratings of the converters are not exceeded.

3.2 Control scheme

We propose a distributed control scheme composed of $N-1$ subcontrollers, one for each HVDC converter except converter N which maintains the voltage of the DC grid. The subcontroller assigned to converter $i \in \{1, \dots, N-1\}$ modifies the value of P_i^{dc} such that

$$\frac{dP_i^{\text{dc}}}{dt} = \alpha \sum_{j=1}^N b_{ij}(\Delta f_i - \Delta f_j) + \beta \sum_{j=1}^N b_{ij} \left(\frac{df_i}{dt} - \frac{df_j}{dt} \right) \quad (10)$$

where

- $\Delta f_i = f_i - f_{nom,i}$ is the frequency deviation of area i .
- α and β are analogous to the integral control gain and the proportional control gain of a PI controller, respectively. The higher the gains, the closer the areas' frequencies stay to each other when one area experiences a sudden power imbalance. Gain values are limited in practice by (i) the maximal rate of change of power flows through the converter, and (ii) stability considerations of the controlled system, for example, taking delays into account (see [15]).
- b_{ij} 's are the coefficients representing the communication graph between the AC areas. The value of b_{ij} equals 1 if subcontroller i receives frequency information of area j , and 0 otherwise.

The control law for subcontroller i is illustrated in Fig. 2.

The intuition behind the control scheme defined in (10) is as follows. If the frequency deviation of area i is higher (lower, resp.) than the average frequency deviation of the other areas, then more (less, resp.) power should be withdrawn from this area to drive its frequency deviation back towards that of the other areas. The adjustment of this power (P_i^{dc}) is determined by subcontroller i , which is a PI controller whose error signal is the sum of the differences between its own frequency deviation and that of the AC areas from which it obtains information. From a global point of view, the control scheme composed of all the subcontrollers takes the form of an algorithm for the consensus problem. This problem appears in the context of coordination of multi-agent systems: the objective is, for agents performing a collective task in a distributed way (i.e. without a supervisor telling everyone what to do), to exchange and process information in order to reach agreement on quantities of interest that are necessary to coordinate their actions [7, 16]. This framework indeed corresponds to the HVDC interconnection setting. Theoretical results on consensus will therefore provide useful tools for the stability study of our control scheme.

We assume in this paper that the communication channels between the AC areas are delay-free, that is, if one AC area has access to the system information of another area, then

this information is instantaneously available. The effects of time-delays on the control scheme are investigated in another paper by the authors [15].

Remark 1: To comply with Constraints (8) and (9), a saturation function for control variables should be introduced. In most cases, these restrictions do not affect the effectiveness of the control scheme. Indeed, $V_1^{dc}, \dots, V_N^{dc}$ are close to each other under normal operating conditions. However, limitations on $P_1^{dc}, \dots, P_N^{dc}$ could indeed significantly limit the degree of primary reserve sharing. This impact could be compared with that of the maximum current limits on AC tie lines.

4 Stability analysis of the control scheme

This section reports a theoretical study on the stability properties of the control scheme. We first characterise the unique equilibrium point of a system subjected to a power imbalance in one AC area. Then, we elaborate on the conditions under which the system converges to that equilibrium point, and we prove stability for the particular case where all the AC areas have identical parameters.

The stability analysis relies on the following assumptions:

Assumption 1: The losses within the DC grid do not vary with time, that is

$$\sum_{i=1}^N \frac{dP_i^{dc}}{dt} = 0 \tag{11}$$

Remark 2: Assumption 1 is justifiable for the reason that the losses in the DC grid are small compared to the power exchanged in the grid, and that the variations of these losses are still smaller compared to the total losses when $P_1^{dc}, \dots, P_{N-1}^{dc}$ vary according to (10).

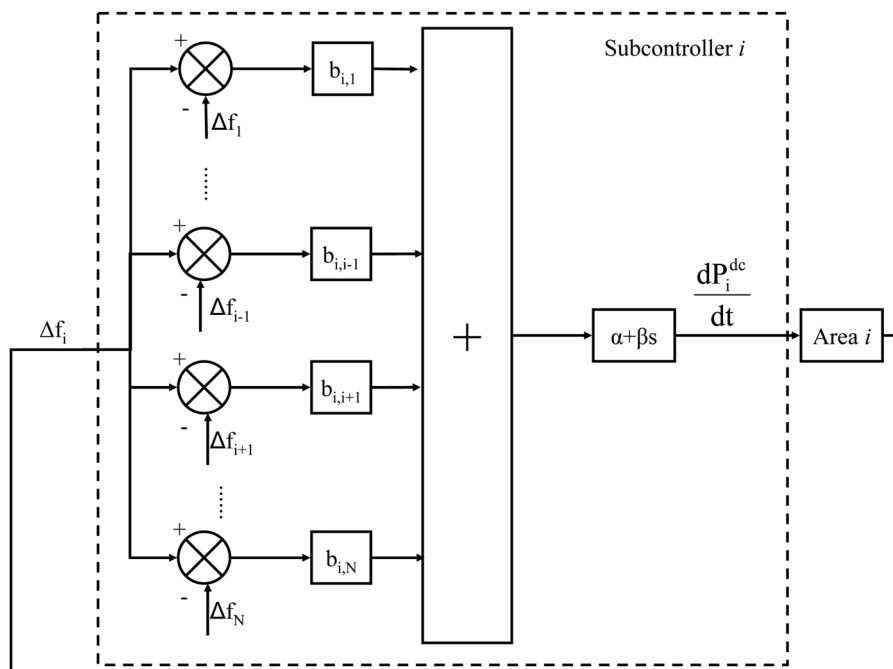


Fig. 2 Diagram of the control law for subcontroller i

Assumption 2: The communication graph that represents the frequency information availability at different subcontrollers has the following properties:

- The communication graph is constant in time.
- The communication graph is connected, that is, if $b_{ij} = 0$, then there must exist some intermediate indices k_1, \dots, k_m such that $b_{ik_1} = b_{k_1 k_2} = \dots = b_{k_m j} = 1$.
- The communication graph is undirected, that is, if the subcontroller of one area has access to the frequency information of another area, then the subcontroller of this second area also has access to the frequency information of the first one, that is, if $b_{ij} = 1$ then $b_{ji} = 1$, $\forall i, j \in \{1, \dots, N - 1\}$.

Assumption 3: The non-linear equation resulting from (5)–(7) can be linearised around $f_i = f_{\text{nom},i}$ as

$$2\pi J_i \frac{df_i}{dt} = \frac{P_{mi} - P_{li}^o - P_i^{\text{dc}}}{2\pi f_{\text{nom},i}} - 2\pi D_i (f_i - f_{\text{nom},i}) \quad (12)$$

where $D_i = D_{gi} + \bar{P}_{li}^o D_{li} / (4\pi^2 f_{\text{nom},i})$, with \bar{P}_{li}^o being the value of P_{li}^o at the equilibrium point around which the linearisation is carried out.

It is important to note that, under Assumptions 1 and 2, the dynamics of P_N^{dc} to satisfy (11) are the same as described by (10), where $b_{Ni} = b_{iN}$, $\forall i \in \{1, \dots, N\}$. In the following, the HVDC system is thus modelled by a linear system, where the dynamics of area $i \in \{1, \dots, N\}$ are defined by (1), (12) and controller (10).

4.1 Equilibrium point

Proposition 1: Consider that the HVDC system, initially operating at its nominal equilibrium, is suddenly subjected to a step change in the load demand of one of its AC areas. Then, under Assumptions 1, 2 and 3, the (linearised) HVDC system has a unique equilibrium point, at which the frequency deviations of all AC areas are equal.

Proof: Prior to the step change in the load demand of one AC area, each area is considered in steady state with its frequency regulated at $f_{\text{nom},i}$. We denote these steady-state values by the variables with a bar overhead. After the step change in the load, the variables start to change. We introduce the following incremental variables

$$x_i(t) = f_i(t) - \bar{f}_{\text{nom},i}$$

$$y_i(t) = P_{mi}(t) - \bar{P}_{mi}$$

$$u_i(t) = P_i^{\text{dc}}(t) - \bar{P}_i^{\text{dc}}$$

$$v_i(t) = P_{li}^o(t) - \bar{P}_{li}^o$$

By introducing these variables, (1), (10) and (12) become

$$\frac{dx_i(t)}{dt} = -a_{1i}x_i(t) + a_{2i}y_i(t) - a_{2i}u_i(t) - a_{2i}v_i(t) \quad (13)$$

$$\frac{dy_i(t)}{dt} = -a_{3i}x_i(t) - a_{4i}y_i(t) \quad (14)$$

$$\frac{du_i(t)}{dt} = \alpha \sum_{j=1}^N b_{ij}(x_i(t) - x_j(t)) + \beta \sum_{j=1}^N b_{ij} \left(\frac{dx_i(t)}{dt} - \frac{dx_j(t)}{dt} \right) \quad (15)$$

where $a_{1i} = D_i/J_i$, $a_{2i} = 1/(4\pi^2 f_{\text{nom},i} J_i)$, $a_{3i} = P_{\text{nom},i}/(T_{\text{smi}} \sigma f_{\text{nom},i})$ and $a_{4i} = 1/T_{\text{smi}}$. Note that a_{1i} , a_{2i} , a_{3i} and a_{4i} are all positive constants.

Equations (13)–(15) describe the closed-loop dynamics of AC area i , where the state variables are $x_i(t)$, $y_i(t)$, $u_i(t)$, and the external input is $v_i(t)$. Initially, all the state variables are equal to zero, since they are defined as the incremental values with respect to the initial nominal equilibrium. At t_0 , a step change in load occurs in area m such that

$$v_i(t) = \begin{cases} \bar{v}_m & \text{for } i = m \text{ and } t > t_0 \\ 0 & \text{otherwise} \end{cases} \quad (16)$$

We now search for equilibrium points of the system following the step change in $v_m(t)$. Let (x_i^e, y_i^e, u_i^e) characterise the state of area i at such an equilibrium point. At this point

$$\frac{dx_i(t)}{dt} = \frac{dy_i(t)}{dt} = \frac{du_i(t)}{dt} = 0 \quad (17)$$

Thus, (13)–(15) become algebraic equations

$$0 = -a_{1i}x_i^e + a_{2i}y_i^e - a_{2i}u_i^e - a_{2i}v_i(t > t_0) \quad (18)$$

$$0 = -a_{3i}x_i^e - a_{4i}y_i^e \quad (19)$$

$$0 = \alpha \sum_{j=1}^N b_{ij}(x_i^e - x_j^e) \quad (20)$$

Equation (20) can be written in matrix form for the entire HVDC system. Define the vector $x^e = [x_1^e, \dots, x_N^e]^T$ and let $\mathbf{0}_N$ ($\mathbf{1}_N$, resp.) denote the column vector of length N with all components equal to 0 (1, resp.). Then, Equation (20) becomes

$$\mathbf{0}_N = \alpha \mathbf{L} x^e \quad (21)$$

where \mathbf{L} is the Laplacian matrix of the communication graph. It is defined by

$$[\mathbf{L}]_{ij} = \begin{cases} -b_{ij} & \text{for } i \neq j \\ \sum_{j \neq i} b_{ij} & \text{for } i = j \end{cases} \quad (22)$$

The Laplacian matrix \mathbf{L} of a communication graph satisfying Assumption 2 is symmetric positive semi-definite and its only zero eigenvalue corresponds to the eigenvector $\mathbf{1}_N$. Therefore equilibrium requires that the frequency deviations of all AC areas be equal. Let x^e be the value of this common frequency deviation at the equilibrium point. From (18) and (19), we obtain

$$y_i^e = -\frac{a_{3i}}{a_{4i}} x^e \quad (23)$$

$$u_i^e = -\left(\frac{a_{1i}}{a_{2i}} + \frac{a_{3i}}{a_{4i}}\right)x^e - v_i(t > t_0)$$

$$= \begin{cases} -\left(\frac{a_{1m}}{a_{2m}} + \frac{a_{3m}}{a_{4m}}\right)x^e - \bar{v}_m & \text{for } i = m \\ -\left(\frac{a_{1i}}{a_{2i}} + \frac{a_{3i}}{a_{4i}}\right)x^e & \text{otherwise} \end{cases} \quad (24)$$

We see in the above expressions that if x^e can be uniquely determined, then the equilibrium point exists and is unique. In fact, Assumption 1 implies that $\sum_{i=1}^N u_i(t)$ remains constant, and the initial conditions yield that $\sum_{i=1}^N u_i(0) = 0$. Thus

$$\sum_{i=1}^N u_i^e = 0 \quad (25)$$

From (24), we see that x^e is uniquely determined as

$$x^e = -\bar{v}_m \cdot \left(\sum_{i=1}^N \frac{a_{1i}a_{4i} + a_{2i}a_{3i}}{a_{2i}a_{4i}}\right)^{-1} \quad (26)$$

□

Remark 3: We considered above that the step change in the load occurs in only one AC area. However, for the general case where $v_i(t)$ changes in more than one area and eventually settles at \bar{v}_i different from 0, it is straightforward to extend the above results to reach a similar conclusion on the existence of a unique equilibrium point, with x^e given by

$$x^e = -\left(\sum_{i=1}^N \bar{v}_i\right) \left(\sum_{i=1}^N \frac{a_{1i}a_{4i} + a_{2i}a_{3i}}{a_{2i}a_{4i}}\right)^{-1} \quad (27)$$

Remark 4: A physical interpretation for the different components of the equilibrium point can be found. Indeed, from (23) and (24), we have

$$\sum_{i=1}^N y_i^e = \sum_{i=1}^N \bar{v}_i + \sum_{i=1}^N u_i^e - \left(\sum_{i=1}^N \frac{a_{1i}}{a_{2i}}\right)x^e \quad (28)$$

where $\sum_{i=1}^N y_i^e$ is the total change in the mechanical power because of primary frequency control of all areas; $\sum_{i=1}^N \bar{v}_i$ is the total change in the load demand; $\sum_{i=1}^N u_i^e$ is the total change in the losses within the DC grid, and it equals 0, see (25); and $(\sum_{i=1}^N a_{1i}/a_{2i})x^e$ contains the damping effects of the generators and the loads resulted from non-zero frequency deviations.

In practice, the order of magnitude of $(\sum_{i=1}^N a_{1i}/a_{2i})x^e$ is much smaller than that of $\sum_{i=1}^N \bar{v}_i$, which means that the final variation in the mechanical power induced by primary frequency control of all the areas is approximately equal to the total variation in the load.

Having computed the equilibrium of the system as a function of \bar{v}_i , we make the final change of variables

$$x_{\text{new},i}(t) = x_i(t) - x^e$$

$$y_{\text{new},i}(t) = y_i(t) - y_i^e$$

$$u_{\text{new},i}(t) = u_i(t) - u_i^e$$

$i = 1, \dots, N$. Define the vectors

$$\mathbf{x}_{\text{new}}(t) = [x_{\text{new},1}(t), \dots, x_{\text{new},N}(t)]^T$$

$$\mathbf{y}_{\text{new}}(t) = [y_{\text{new},1}(t), \dots, y_{\text{new},N}(t)]^T$$

$$\mathbf{u}_{\text{new}}(t) = [u_{\text{new},1}(t), \dots, u_{\text{new},N}(t)]^T$$

and the matrices $A_i = \text{diag}(a_{1i}, \dots, a_{Ni}), i = 1, 2, 3, 4$. Then, the dynamics of the linear system for variables $\mathbf{x}_{\text{new}}, \mathbf{y}_{\text{new}}, \mathbf{u}_{\text{new}}$ are given by

$$\frac{d}{dt} \begin{pmatrix} \mathbf{x}_{\text{new}} \\ \mathbf{y}_{\text{new}} \\ \mathbf{u}_{\text{new}} \end{pmatrix} = \begin{pmatrix} -A_1 & A_2 & -A_2 \\ -A_3 & -A_4 & \mathbf{0} \\ \alpha L - \beta L A_1 & \beta L A_2 & -\beta L A_2 \end{pmatrix} \begin{pmatrix} \mathbf{x}_{\text{new}} \\ \mathbf{y}_{\text{new}} \\ \mathbf{u}_{\text{new}} \end{pmatrix}$$

$$\doteq \mathbf{M} \begin{pmatrix} \mathbf{x}_{\text{new}} \\ \mathbf{y}_{\text{new}} \\ \mathbf{u}_{\text{new}} \end{pmatrix} \quad (29)$$

The stability of this system – and thus the convergence property of the system towards equal frequency deviations when subjected to small load variations – can be inferred from the eigenvalues of \mathbf{M} . It is not difficult to see that \mathbf{M} will always have one zero eigenvalue, associated to the

eigenvector $\begin{pmatrix} \mathbf{1}_{N'} \\ A_4^{-1} A_3 \mathbf{1}_{N'} \\ (A_2^{-1} A_1 + A_4^{-1} A_3) \mathbf{1}_{N'} \end{pmatrix}$. The strict zero

eigenvalue corresponds to a continuum of equilibria with different values of $\sum_{i=1}^N u_i$. This direction of variation can be ignored since Assumption 1 guarantees that the system under contingency keeps a constant value of $\sum_{i=1}^N u_i(t)$, see the proof of Proposition 1. As a conclusion, \mathbf{M} has one 0 eigenvalue which is irrelevant given Assumption 1, and stability is dictated by its $3N-1$ remaining eigenvalues.

For a given particular MT-HVDC system, the eigenvalues of \mathbf{M} can be computed numerically. The system with our control scheme is then proven to be locally exponentially stable if \mathbf{M} has one zero eigenvalue (shift of equilibrium point, see previous paragraph) and $3N-1$ eigenvalues with negative real part. However, it is not clear a priori for which values of α and β (if there exist any) this is achieved. In the next subsection, we propose a first step towards a full theoretical stability analysis by considering the special case where all AC areas have identical parameters, that is

$$A_i = a_i \mathbf{I}_N, \quad i = 1, 2, 3, 4 \quad (30)$$

where \mathbf{I}_N is the $N \times N$ identity matrix.

4.2 Stability of the system with identical AC areas

Proposition 2: Consider that all the AC areas of the HVDC system have identical parameters, and that Assumptions 1, 2 and 3 are satisfied. Then, the unique equilibrium with equal frequency deviations given by (23), (24) and (27) is exponentially stable for the MT-HVDC model with the control scheme defined in (10) for any $\alpha > 0$ and $\beta \geq 0$.

Proof: Under Assumption 2, the Laplacian \mathbf{L} of the communication graph is positive semi-definite and has eigenvalues such that $0 = \lambda_1 < \lambda_2 \leq \dots \leq \lambda_N$. Let \mathbf{U} be an

orthogonal matrix such that

$$U^{-1}LU = \text{diag}(\lambda_1, \dots, \lambda_N) \doteq \tilde{L} \quad (31)$$

Then we have

$$(\mathbf{I}_3 \otimes U^{-1})\mathbf{M}(\mathbf{I}_3 \otimes U) = \begin{pmatrix} -a_1\mathbf{I}_N & a_2\mathbf{I}_N & -a_2\mathbf{I}_N \\ -a_3\mathbf{I}_N & -a_4\mathbf{I}_N & \mathbf{0} \\ \alpha\tilde{L} - \beta a_1\tilde{L} & \beta a_2\tilde{L} & -\beta a_2\tilde{L} \end{pmatrix} \doteq \tilde{\mathbf{M}} \quad (32)$$

and $\tilde{\mathbf{M}}$ has the same eigenvalues as \mathbf{M} . By simple reordering of rows and columns, $\tilde{\mathbf{M}}$ can further be brought into block-diagonal form where each block takes the form

$$\tilde{\mathbf{M}}_i = \begin{bmatrix} -a_1 & a_2 & -a_2 \\ -a_3 & -a_4 & 0 \\ \alpha\lambda_i - \beta a_1\lambda_i & \beta a_2\lambda_i & -\beta a_2\lambda_i \end{bmatrix} \quad (33)$$

one for each eigenvalue of \mathbf{L} .

For $i = 1$, we have $\lambda_1 = 0$, which gives the zero eigenvalue associated to equilibrium shift, and covered by Assumption 1. The two remaining eigenvalues of $\tilde{\mathbf{M}}_1$ are those of the matrix $\begin{bmatrix} -a_1 & a_2 \\ -a_3 & -a_4 \end{bmatrix}$. Since the constants a_1, a_2, a_3, a_4 are all positive as defined earlier, the eigenvalues associated to $\tilde{\mathbf{M}}_1$ must have negative real part.

Let ξ_k denote an eigenvalue of $\tilde{\mathbf{M}}_i$ for $i > 1$. To find it, we write

$$\det(\xi_k \mathbf{I}_3 - \tilde{\mathbf{M}}_i) = \xi_k^3 + (a_1 + a_4 + \beta a_2 \lambda_i) \xi_k^2 + (a_1 a_4 + a_2 a_3 + \alpha a_2 \lambda_i + \beta a_2 a_4 \lambda_i) \xi_k + \alpha a_2 a_4 \lambda_i \quad (34)$$

By the Routh–Hurwitz stability criterion for negativity of polynomial roots, all ξ_k will have negative real part if, for all $i > 1$

$$(a_1 + a_4 + \beta a_2 \lambda_i) > 0 \quad (35)$$

$$(a_1 + a_4 + \beta a_2 \lambda_i)(a_1 a_4 + a_2 a_3 + \alpha a_2 \lambda_i + \beta a_2 a_4 \lambda_i) - \alpha a_2 a_4 \lambda_i > 0 \quad (36)$$

$$\alpha a_2 a_4 \lambda_i > 0 \quad (37)$$

Given the positiveness of the coefficients a_1, a_2, a_3, a_4 defined in Section 4.1, the above inequalities are satisfied for all $\lambda_i > 0$ as long as $\alpha > 0$ and $\beta \geq 0$. This completes the proof. \square

Remark 5: If we choose $\beta = 0$, then the system will converge at a slow pace dictated by the system’s dissipation. Taking $\beta > 0$ introduces a dissipation-like term in the controller and therefore allows much faster and less oscillatory convergence to equal frequency deviations.

Remark 6: Note that the controller gains α and β are always multiplied by the graph connectivity eigenvalue λ_i in (34). The slowest convergence rate will therefore be dictated by the smallest Laplacian eigenvalue, λ_2 . The latter is an extensively studied object of graph theory, where it is called the algebraic graph connectivity. This should allow

evaluating which graphs are more or less favourable (i.e. require smaller or larger gains in our controller) for synchronisation of frequency deviations.

The study reported hereabove shows that an MT-HVDC system with identical AC areas is exponentially stable when applying our control scheme. This theoretical study relies on some simplifying assumptions. However, the obtained exponential stability property is robust to small errors in the system dynamics, which indicates that the result should indeed hold on real systems with non-linear dynamics and non-identical AC areas, as long as the disturbances are small enough and the dissimilarities between the AC areas are small enough. The next section further illustrates this fact with numerical simulations.

5 Simulations

In this section, the control scheme is applied to a benchmark system that has a five-terminal HVDC system. First, we fully describe the benchmark system. Then, we report and discuss simulation results.

5.1 Benchmark system and contingency

The benchmark system is made of five non-synchronous areas, connected by a five-terminal HVDC system. The converter of area 5 is chosen to regulate the DC voltage, whose setting is 100 kV. The topology of the interconnected system is represented in Fig. 3. The communication graph coincides with the DC network topology. The DC resistances between the AC areas are: $R_{12} = 1.39 \Omega$, $R_{15} = 4.17 \Omega$, $R_{23} = 2.78 \Omega$, $R_{25} = 6.95 \Omega$, $R_{34} = 2.78 \Omega$ and $R_{45} = 2.78 \Omega$. In contrast to the stability analysis in Section 4.2, the simulations consider AC areas with different parameters, as summarised in Table 1. The initial values of the DC-grid variables are also included in this table. The AC areas are simulated with the full non-linear model described by (1), (5), (6), (7) and (10). For the DC grid, we use (4) to calculate the DC load flow instead of making Assumption 1.

The continuous-time differential equations are integrated using an Euler method with a time-discretisation step of 1 ms. To observe the system’s response to a power imbalance, we assume that all the areas initially operate in steady state at the nominal frequency. Then at time $t = 2$ s, a step increase by 5% of the value of P_{12}^o (see (6)) is considered.

5.2 Results

Fig. 4 gives the evolution of the frequencies when the controller gains are chosen as $\alpha = \beta = 2 \times 10^6$. For

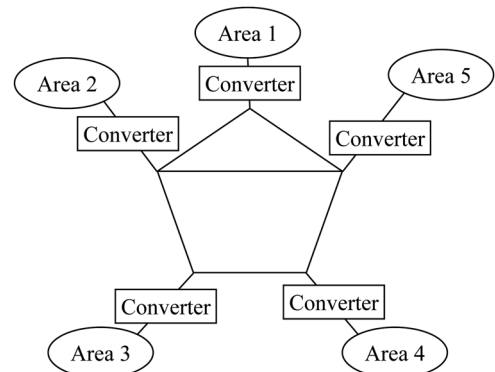


Fig. 3 Interconnected system topology of the benchmark system

Table 1 Parameter values for the AC areas and initial values of the DC-grid variables

	Area					Unit
	1	2	3	4	5	
f_{nom}	50	50	50	50	50	Hz
P_m^o	50	80	50	30	80.4	MW
P_{nom}	50	80	50	30	80.4	MW
J	2026	6485	6078	2432	4863	kg m ²
D_g	48.4	146.4	140	54.7	95.1	W s ²
σ	0.02	0.04	0.06	0.04	0.03	(dimensionless)
T_{sm}	1.5	2.0	2.5	2	1.8	s
P_i^o	100	60	40	50	40	MW
D_i	0.01	0.01	0.01	0.01	0.01	s
\bar{P}^{dc}	-50	20	10	-20	40.4	MW
\bar{V}^{dc}	99.17	99.60	99.73	99.59	100	kV

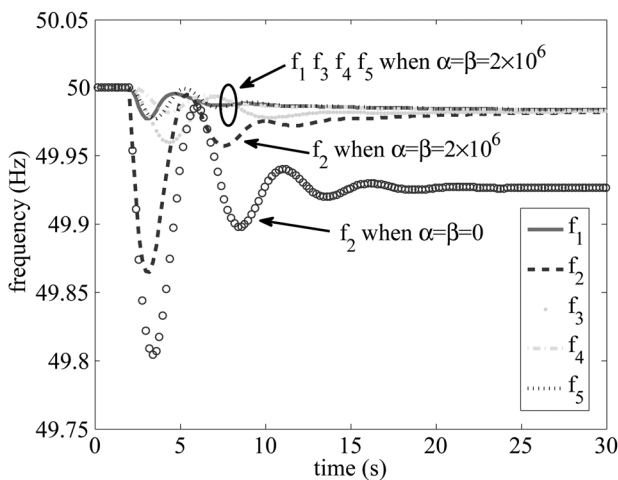


Fig. 4 Frequencies of the five AC areas under the control scheme when $\alpha = \beta = 2 \times 10^6$. f_2 when the primary reserves are not shared is also shown

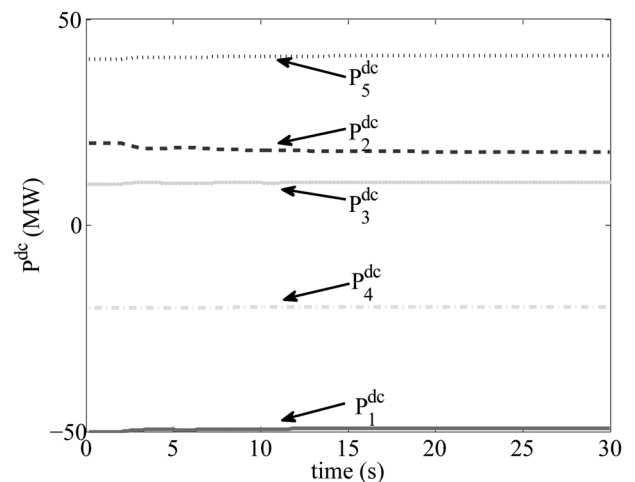


Fig. 5 Power injections from the five AC areas into the DC grid when $\alpha = \beta = 2 \times 10^6$

comparison, we also show in the same figure the frequency of area 2 when the distributed control scheme is not applied (i.e. with $P_1^{dc}, \dots, P_5^{dc}$ kept constant). The simulations show that without the control scheme, the frequency of area 2 undergoes a deviation with transient maximum of 0.196 Hz and stabilises at 49.927 Hz. When the control scheme is applied, the maximum transient deviation of area 2 drops to 0.136 Hz, and the frequencies of the five areas converge to each other to finally settle at 49.983 Hz. Fig. 5 shows the evolution of $P_1^{dc}, \dots, P_5^{dc}$ expressed in MW. P_2^{dc} is the power injection which varies the fastest. In particular, it decreases by 5% in the 2 s following the load step increase. For information, Fig. 6 shows the DC voltages of the converters, whose variations because of the control scheme are small with respect to their absolute values. In particular, the band of variation of each voltage remain separate from each other, except those of V_2^{dc} and V_4^{dc} .

The above results show that our control scheme leads to a significant improvement in the steady-state frequency deviation of area 2, from 0.073 to 0.017 Hz. However, the transient performance is quite poor, since the maximum transient deviation is just slightly reduced from 0.196 to 0.136 Hz. To improve the transient performance, we increase the controller gains. For the sake of simplicity, we impose that $\alpha = \beta$. Figs. 7 and 8 shows the frequencies when the controller gains are increased to $\alpha = \beta = 1 \times 10^7$.

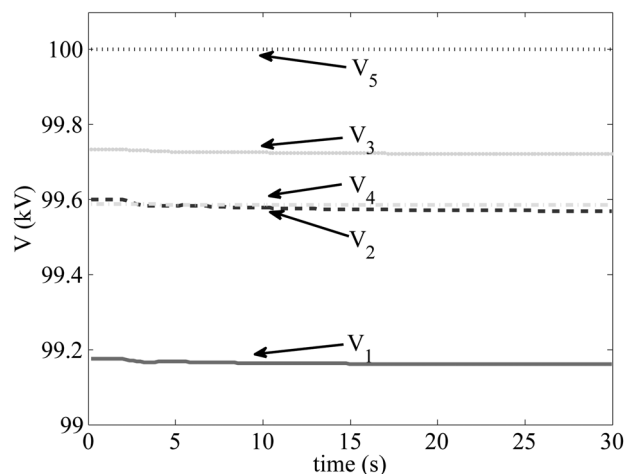


Fig. 6 DC voltages of the converters when $\alpha = \beta = 2 \times 10^6$

Compared to Fig. 4, the transient behaviour is significantly improved with the larger controller gains: the frequencies of all the areas converge to each other more quickly; the maximal transient deviation of area 2 is reduced to 0.075 Hz, whereas the steady-state equilibrium does not change, as suggested by Proposition 1. The improvement in the

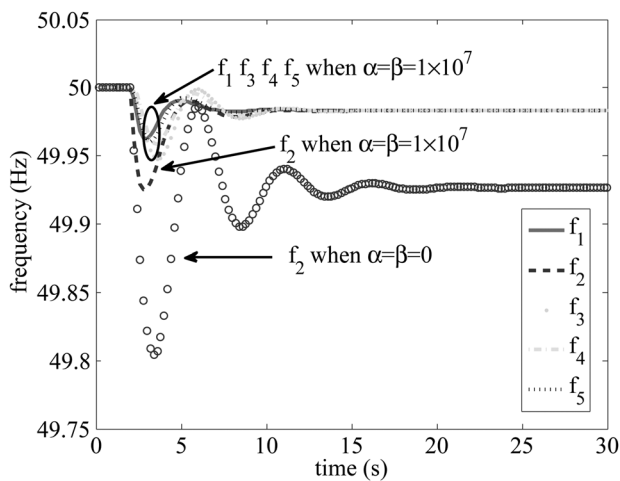


Fig. 7 Frequencies of the five AC areas under the control scheme when $\alpha = \beta = 1 \times 10^7$. f_2 when the primary reserves are not shared is also shown

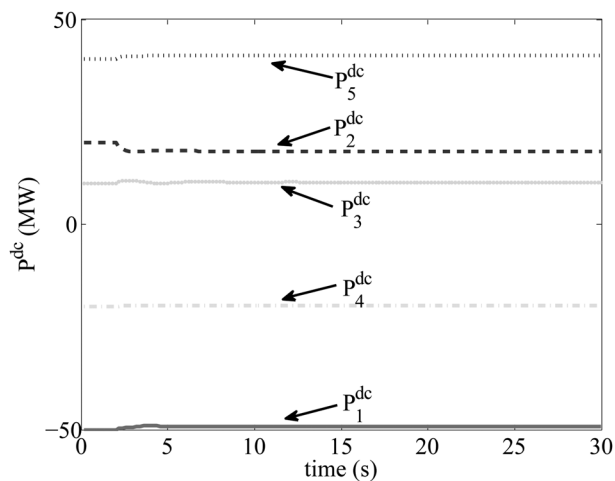


Fig. 8 Power injections from the five AC areas into the DC grid when $\alpha = \beta = 1 \times 10^7$

transient behaviour comes at the price of faster variations of the power injections, which are shown in Fig. 8. In this case, P_2^{dc} decreases by 10% within 0.6 s after the load step increase. Nevertheless, even for these larger controller gains, the variations in P_i^{dc} remain moderately small. From an engineering point of view, the power injection variations shown in the figures are within modern converters' power-tracking speed, as shown in other studies such as [17, 18]. The DC voltages of the converters in this case, which are not given in this paper, differ little from Fig. 6.

In the simulations, we have considered that the primary reserve of each generator was equal to its initial power output. For the case of smaller reserves, additional simulations not reported in the paper show that the frequencies still converge even if some areas have reached their primary reserve limits. However, when the primary reserves of all areas are depleted, generators are unable to restore the overall power balance and all the frequencies would keep decreasing, until they reach a certain threshold that triggers emergency control actions such as load-shedding in a real power system.

6 Conclusions and future work

In this paper, we presented a control scheme to share primary reserves among non-synchronous AC areas connected by an MT-HVDC system. With this control scheme, in response to a power imbalance in one area, all the areas modify their power injections into the DC grid in a coordinated way so that their frequency deviations converge to each other. A theoretical study indicates that, under some assumptions, the interconnected system is stable and, following a power imbalance in one area, converges towards a new equilibrium with identical frequency deviations in all the areas. Simulations on a benchmark system with five non-identical AC areas show that with a proper choice of the controller gains, the frequency deviations of all the areas rapidly converge to each other following a step change in the load demand. These simulations, together with others not reported in this paper, highlight that our control scheme can make good use of the fast power-tracking capability of HVDC converters to coordinate primary frequency control efforts among non-synchronous AC areas.

This control scheme can be improved along several lines. One way of improvement could be to choose different gains for the subcontrollers, or even let them vary on-line in accordance with the operational conditions of the areas, so that other factors can be taken into account. For example, the relative size of one area with respect to others can be considered, so that in response to a major power imbalance in a larger area, a smaller area with less primary reserves can choose to stop sharing its own reserve if it judges that a further sharing of its reserve would jeopardise its own stability. In this way, the HVDC system would still play the role of 'firewall' that prevents cascading outages across AC areas. Another way of improvement would be to adapt the control scheme so as to compensate for the time needed for the subcontroller to gather the frequency information of other areas. Indeed, compensating for these time-delays is important since as shown in another paper of the authors [15], they may lead to undamped frequency oscillations. It is also possible to propose control schemes that avoid explicit communication between the AC areas, and nevertheless allow some sharing of primary reserves, see for example [19–22].

7 Acknowledgments

While working on this topic, Alain Sarlette was a postdoctoral researcher at Mines ParisTech and at FRS-FNRS, University of Liège. Damien Ernst thanks the FRS-FNRS for its financial support. These authors also thank the financial support of the Belgian Network DYSCO, an Interuniversity Attraction Poles Programme initiated by the Belgian State, Science Policy Office. Y. Phulpin was with SUPELEC when completing part of his contribution to the paper.

8 References

- 1 Rebours, Y.G., Kirschen, D.S., Trotignon, M., Rossignol, S.: 'A survey of frequency and voltage control ancillary services – part I: technical features', *IEEE Trans. Power Syst.*, 2007, **22**, (1), pp. 350–357
- 2 Grünbaum, R., Halvarsson, B., Wilk-Wilczynski, A.: 'FACTS and HVDC light for power system interconnections'. Proc. Power Delivery Conf., Madrid, Spain, September 1999, pp. 1–18
- 3 Bahrman, M.P., Johnson, B.K.: 'The ABCs of HVDC transmission technology', *IEEE Power Energy Mag.*, 2007, **5**, (2), pp. 32–44

- 4 Papadogiannis, K., Hatziaargyriou, N.: 'Optimal allocation of primary reserve services in energy markets', *IEEE Trans. Power Syst.*, 2004, **19**, (1), pp. 652–659
- 5 de Toledo, P., Pan, J., Srivastava, K., Wang, W., Hong, C.: 'Case study of a multi-infeed HVDC system'. Proc. Joint Int. Conf. on Power System Technology and IEEE Power India Conf., New Delhi, India, October 2008, pp. 1–7
- 6 Fujita, G., Shirai, G., Yokoyama, R.: 'Automatic generation control for DC-link power system'. Proc. IEEE/PES Transmission and Distribution Conf. and Exhibition: Asia Pacific, October 2002, vol. 3, pp. 1584–1588
- 7 Olfati-Saber, R., Fax, J., Murray, R.: 'Consensus and cooperation in networked multi-agent systems', *Proc. IEEE*, 2007, **95**, (1), pp. 215–233
- 8 ENTSO-E: 'UCTE operation handbook' (ENTSO-E, Brussels, 2004)
- 9 Kundur, P.: 'Power system stability and control' (McGraw-Hill, New York, 1994)
- 10 Ourari, M.L., Dessaint, L.-A., Do, V.Q.: 'Generating units aggregation for dynamic equivalent of large power systems'. Proc. IEEE PES General Meeting, June 2004, vol. 2, pp. 1535–1541
- 11 Grigsby, L.L.: 'Power system stability and control' (The Electrical Engineering Handbook Series), (CRC Press Inc., Boca Raton, 2007)
- 12 Lescale, V.F., Kumar, A., Juhlin, L.-E., Bjorklund, H., Nyberg, K.: 'Challenges with multi-terminal UHVDC transmissions'. Proc. Joint Int. Conf. on Power System Technology and IEEE Power India Conf., New Delhi, India, October 2008, pp. 1–7
- 13 Jiang, H., Ekström, A.: 'Multiterminal HVDC system in urban areas of large cities', *IEEE Trans. Power Deliv.*, 1998, **13**, (4), pp. 1278–1284
- 14 Xu, L., Williams, B., Yao, L.: 'Multi-terminal DC transmission systems for connecting large offshore wind farms'. Proc. IEEE PES General Meeting – Conversion and Delivery of Electrical Energy in the 21st Century, Pittsburgh, PA, July 2008, pp. 1–7
- 15 Dai, J., Phulpin, Y., Sarlette, A., Ernst, D.: 'Impact of delays on a consensus-based primary frequency control scheme for AC systems connected by a multi-terminal HVDC grid'. Proc. IREP Symp. – Bulk Power Systems Dynamics and Control – VIII, Buzios, Rio de Janeiro, Brazil, August 2010, pp. 1–9
- 16 Fax, J.A., Murray, R.M.: 'Information flow and cooperative control of vehicle formations', *IEEE Trans. Autom. Control*, 2004, **49**, (9), pp. 1465–1476
- 17 Meah, K., Ula, A.H.M.S.: 'A new simplified adaptive control scheme for multi-terminal HVDC transmission systems', *Int. J. Electr. Power Energy Syst.*, 2010, **32**, (4), pp. 243–253
- 18 Padiyar, K.R., Prabhu, N.: 'Modelling, control design and analysis of VSC based HVDC transmission systems'. Proc. Int. Conf. on Power System Technology, Singapore, November 2004, vol. 1, pp. 774–779
- 19 Dai, J., Phulpin, Y., Sarlette, A., Ernst, D.: 'Voltage control in an HVDC system to share primary frequency reserves between non-synchronous areas'. Proc. PSCC, Stockholm, Sweden, August 2011, pp. 1–8
- 20 Phulpin, Y.: 'Communication-free inertia and frequency control for wind generators connected by an HVDC-link', *IEEE Trans. Power Syst.*, 2012, **27**, 2 pages
- 21 Moreira, C.L., Silva, B., Soares, F.J., Seca, L., Peças Lopes, J.A.: 'Inertial control in off-shore wind farms connected to AC networks through multi-terminal HVDC grids with VSC'. Proc. CIGRE Int. Symp., Bologna, Italy, 2011, pp. 1–6
- 22 Haileselassie, T.M., Torres-Olguin, R.E., Vrana, T.K., Uhlen, K., Undeland, T.: 'Main grid frequency support strategy for VSC-HVDC connected wind farms with variable speed wind turbines'. Proc. PowerTech, Trondheim, Norway, June 2011, pp. 1–6